



UNIVERSITÀ POLITECNICA DELLE MARCHE
Repository ISTITUZIONALE

Use of acoustic techniques to analyse interlayer shear-torque fatigue test in asphalt mixtures

This is the peer reviewed version of the following article:

Original

Use of acoustic techniques to analyse interlayer shear-torque fatigue test in asphalt mixtures / Ragni, D.; Takarli, M.; Petit, C.; Graziani, A.; Canestrari, F.. - In: INTERNATIONAL JOURNAL OF FATIGUE. - ISSN 0142-1123. - ELETTRONICO. - 131:(2020). [10.1016/j.ijfatigue.2019.105356]

Availability:

This version is available at: 11566/276102 since: 2024-04-29T13:23:50Z

Publisher:

Published

DOI:10.1016/j.ijfatigue.2019.105356

Terms of use:

The terms and conditions for the reuse of this version of the manuscript are specified in the publishing policy. The use of copyrighted works requires the consent of the rights' holder (author or publisher). Works made available under a Creative Commons license or a Publisher's custom-made license can be used according to the terms and conditions contained therein. See editor's website for further information and terms and conditions.

This item was downloaded from IRIS Università Politecnica delle Marche (<https://iris.univpm.it>). When citing, please refer to the published version.

(Article begins on next page)

Use of acoustic techniques to analyse interlayer shear-torque fatigue test in asphalt mixtures

Davide Ragni^{1*}, Mokhfi Takarli², Christophe Petit², Andrea Graziani¹, and Francesco Canestrari¹

¹ *Department of Civil and Building Engineering and Architecture, Università Politecnica delle Marche, via Brecce Bianche, 60131 Ancona, Italy*

² *Laboratoire GC2D, Université de Limoges, Bd J. Derche, 19300 Egletons, France*

* Corresponding author. Tel.: +39 071 220 4780

E-mail address: d.ragni@pm.univpm.it (D. Ragni), mokhfi.takarli@unilim.fr (M. Takarli), christophe.petit@unilim.fr (C. Petit), a.graziani@univpm.it (A. Graziani), f.canestrari@univpm.it (F. Canestrari)

Abstract

Shear-torque tests were used for the first time to assess the fatigue behaviour of double-layered asphalt specimens. During the test, an acoustic emission (AE) technique was used to evaluate the damage process leading to failure. Results showed that the application of cyclic loading led to the decrease of the complex shear modulus, until the physical separation of the two layers. AE analysis showed that damage mostly occurred in the interlayer zone. The comparison between mechanical and AE results suggested that the damage evolution phase occurred when approaching the end of the test when the stiffness decrease was about 70%.

Keywords: asphalt pavements; interlayer bonding; shear-torque fatigue test; acoustic emission; damage evolution.

1. Introduction

Asphalt pavements are multi-layered systems, thus proper interlayer bonding is essential to ensure that the pavement can act as a single structural element in withstanding traffic loading and environmental effects. Inadequate layer bonding may lead to several distresses, like slippage cracking, delamination, distortion, and potholes [1, 2]. Therefore, the service life of multi-layered asphalt pavements strongly depends on the performance of the interface between layers [3].

Testing configurations to investigate interlayer bonding have been categorised into four main groups: torque, direct tension, wedge splitting and direct shear (with or without normal load) [4]. The interlayer performance is typically measured by the interlayer shear strength (ISS) obtained with the monotonic application of a shear load, or displacement, until failure. Although the ISS is not representative of typical in-situ traffic loading conditions, it generally provides a reliable quality assessment of interlayer bonding and is commonly adopted because of its simplicity and the relatively short testing procedure.

In steady flow conditions, traffic loading produces a stress-strain state within the pavement which is cyclic in nature. Thus, the layer interfaces are subjected to shear stress cycles that can lead to damage accumulation phenomena and produce debonding-related distresses. In this sense, cyclic bond testing is expected to lead to the measurement of mechanical parameters that better describe the in-situ behaviour of multi-layered pavement system, in terms of stiffness (small-strain thermo-viscoelasticity) and cumulative damage (e.g. fatigue).

In recent years, several cyclic bond testing devices have been developed following different working schemes [5-8]. Diakhaté et al. [5] developed the double shear test (DST) device to measure the number of loading cycles required to cause failure at the interface. The DST allows the application of a sinusoidal force on a prismatic specimen including two interfaces. Fatigue testing was carried out at one frequency (10 Hz) and two temperatures (10 °C and 20 °C), and the 50% reduction of the initial value of interface shear stiffness was employed as a failure criterion. Boudabbous et al. [9] used the DST device, in both force and displacement control mode, on specimens with notches at the interface. To analyse the fatigue

process, in addition to the conventional approach, the dissipated energy approach was used. Results showed that the change of dissipated energy in each loading cycle could be used as a damage indicator for both damage and failure. Song et al. [7] used a direct shear fatigue device to study the interlayer shear behaviour of systems composed of an open-graded friction course and the underlying layer, with different tack coat application rates. Direct shear fatigue tests were performed using sinusoidal stress at 10 Hz and 20 °C. The 50% reduction of the interface shear stiffness was employed as a failure criterion. Isailović et al. [10] modified the Leutner shear test [11]. Double-layered cylindrical specimens were prepared with and without tack coat application and cyclic shear tests were conducted at different temperatures (from -10 °C to 50 °C) and normal stresses (from 0 MPa to 0.50 MPa). Interlayer shear stiffness, phase angle and dissipated energy were calculated for each test, and the 50% reduction of the interface stiffness was employed as a failure criterion [10].

The literature review shows that shear fatigue failure of multi-layered asphalt specimens subjected to cyclic loading is currently analysed using the same criteria developed for homogeneous specimens [12, 13]. The main disadvantage of this approach is that it is not able to highlight if the damage occurs within the asphalt matrix or is localised at the interlayer. In this context, acoustic emission (AE) techniques could be a useful tool to detect interlayer damage. AE events are elastic waves produced by the rapid release of energy from a localised source within a material. These transient waves can be received and recorded by transducers applied on the surface of the specimen. Counting the AE events is a common way to assess the damage accumulation inside the material. AE techniques have been used to monitor damage evolution in composite materials, wood [14-16] and concrete [17-20]. However, AE applications aimed at characterising the damage progression in asphalt concrete are relatively limited and mainly focused on low-temperature cracking [21, 22].

A first attempt to detect crack initiation and propagation through AE in bituminous mixtures was made by Khosla and Goetz [23]. After performing indirect tensile tests at -23 °C, the experimental results showed that failure happens when a sharp increase in the cumulative AE events is detected. Hesp et al. [24] observed that during restrained cooling tests the AE

activity detected on polymer-modified asphalt mixture is lower than that of the mixture with plain bitumen. Seo and Kim [25] found that the peak of AE events in uniaxial tensile cyclic tests approximately coincides with the macro-crack formation, showing a correlation between AE events and asphalt distresses. Li and Marasteanu [26] used AE measurements to locate the crack propagation in semi-circular bending tests at low temperature for asphalt mixtures (-6 °C, -18 °C and -30 °C). They found that the number of AE events increased as test temperature decreases. Diakhatè et al. [27] performed DST tests on notched asphalt concrete specimens without an interface, in order to guide the shear band localisation and generate the crack from the tip of the notch. Results showed that AE measurements are capable of detecting micro-cracking formation induced by shear loading and that the peak of the cumulative number of AE events corresponds to the transition from micro- to macro-cracks. Moreover, the number of accumulated AE events quickly increased when the 70% reduction of the initial shear modulus was reached.

Given this background, the main objectives of this experimental research were:

- a. to use the AE technique for investigating the damage evolution occurring in double-layered asphalt specimens during shear-torque fatigue tests;
- b. to compare the evolution of stiffness to the accumulation and localisation of the AE events in order to understand the mechanism leading to interface failure;
- c. to improve the interlayer failure criteria based only on stiffness evolution.

To tackle these goals, the torque testing configuration described in a previous study was adopted [28], but it was used for the first time to assess the interlayer bonding properties.

2. Specimen preparation

An asphalt concrete (AC) for surface course with 12.5 mm maximum aggregate size (AC 12.5) was employed in this study. The mixture was prepared with the aggregate gradation shown in Fig. 1 containing basalt coarse aggregate, limestone fine aggregate and filler. The binder was a Styrene-Butadiene-Styrene polymer modified bitumen classified as PMB 45/80-65 [29] and dosed at 5.5% by aggregate mass.

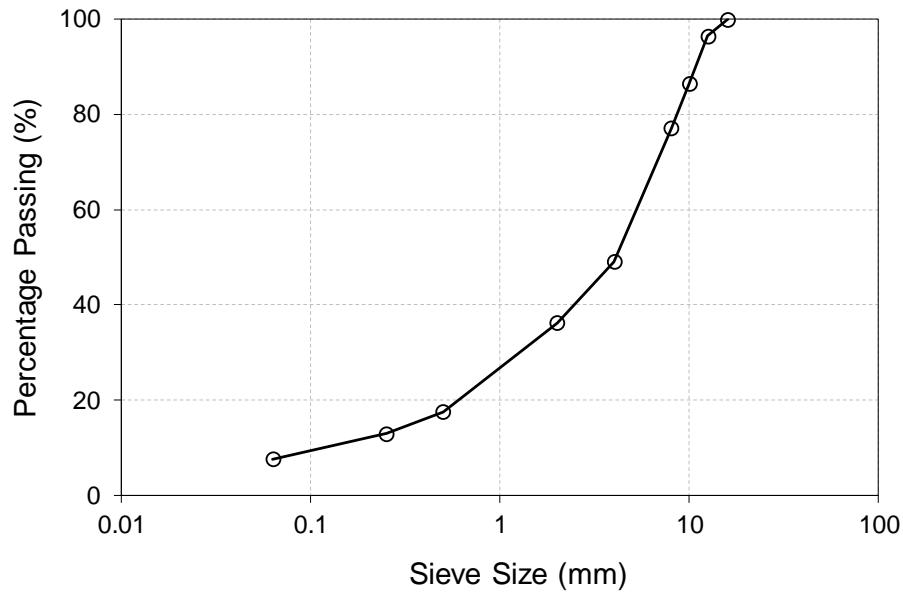
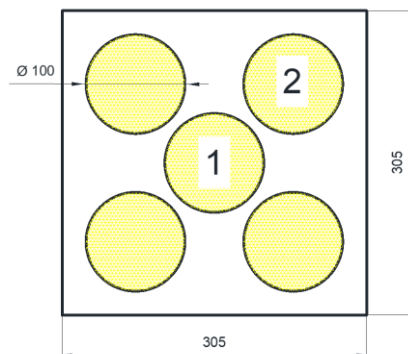


Fig. 1. Grading curve of aggregates.

A double-layered square slab ($305 \times 305 \text{ mm}^2$) was compacted in the laboratory in a stainless-steel mould by means of a roller compactor [30]. The lower layer was compacted at the temperature of 150°C until reaching a target thickness of 60 mm. Then, after cooling at room temperature for 3 hours, the upper layer was compacted at the same temperature reaching a target thickness of 40 mm. A tack coat or reinforcement was not applied at the interface in order to study the failure mechanism in the simplest condition [8]. The slab was demoulded after cooling at room temperature for one day, and five cylindrical specimens, with a nominal diameter of 100 mm, were cored, as shown in Fig. 2. Specimens 1 and 2 were used for this investigation. The upper and lower parts of the specimens were sawed (about 1 cm) and rectified. The final properties of the specimens are summarised in Table 1.



(a)



(b)

Fig. 2. Slab coring procedure: (a) specimen identification and (b) cored cylindrical specimens.

Table 1. Final properties of the specimens.

Specimen	Diameter	Thickness total (H)	Thick. lower layer (h_1)	Thick. upper layer (h_2)	Mass	Bulk density	Air voids
	mm	mm	mm	mm	g	g/cm ³	%
1	99.29	76.72	47.64	29.08	1436.07	2.417	3.11
2	99.38	76.51	47.18	29.33	1436.16	2.420	3.00

3. Testing methods

3.1 Shear-torque fatigue test

The shear-torque configuration was chosen to carry out fatigue tests on double-layered cylindrical specimens. This configuration leads to a non-uniform (i.e. linear) distribution of the shear stress, with the maximum on the outer circumference [4]. This fact does not represent a shortcoming considering that also in the direct shear configuration, the shear stress state at the interface is unknown because distortions occur in the material, due to the specimen clamping system [1]. Moreover, for both configurations, the comparison of the shear stress state to field conditions is extremely difficult, because the actual shear stress distribution at the interface due to vehicular loading is not uniform as well.

Shear-torque fatigue tests were carried out on two double-layered specimens by means of a material testing system (MTS) device equipped with a temperature-controlled chamber. The MTS device is able to apply a torque of 1000 Nm and an axial load of 100 kN. The fatigue tests were performed at a temperature of 20 °C as normally suggested for static tests [4]. A sinusoidal torque with a frequency of 10 Hz and an amplitude T_0 of 85 Nm and 95 Nm was applied on specimens 1 and 2, respectively. An axial compression load N of 0.05 kN was also applied and kept constant during the whole test. The torsional rotation angle was measured using a non-contact angular sensor with an accuracy of 0.001°, located on the upper steel platen as shown by the working scheme in Fig. 3.

Before testing, the cylindrical specimen was glued between two stainless-steel platens using an epoxy resin. The bottom platen was rigidly fixed to the load cell and the upper platen

was connected to an axial-torsional load actuator. A minimum amount of glue was applied to ensure high torsional stiffness and an optimal adhesion between the specimen and the steel platens. After gluing, the specimen was conditioned for 4 hours at 20 °C.

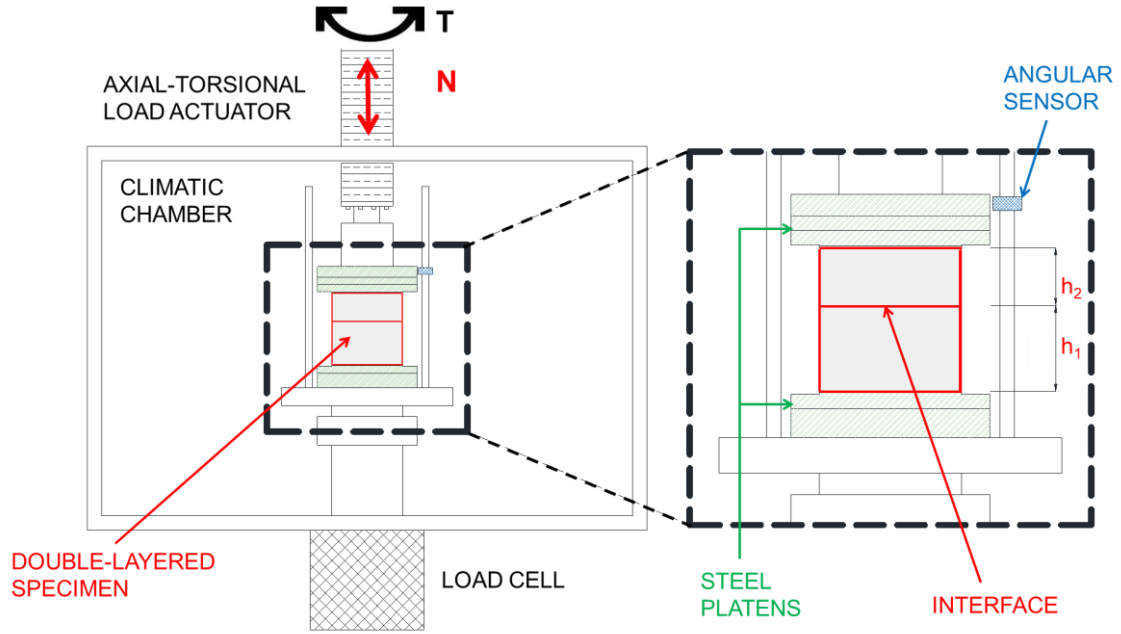


Fig. 3. Working scheme of shear-torque fatigue test.

Fig. 4a shows the coordinate reference system set for the specimen. The X and Y axes lie in a plane located at the interface of the specimen, whereas the Z-axis is perpendicular to the interface plane. Fig. 4b shows a set of recorded data (100 points per cycle) by the load cell and the non-contact angular sensor during cyclic torque tests. The shear-torque fatigue tests were carried out until the physical separation of the upper and the lower layers of the specimen.

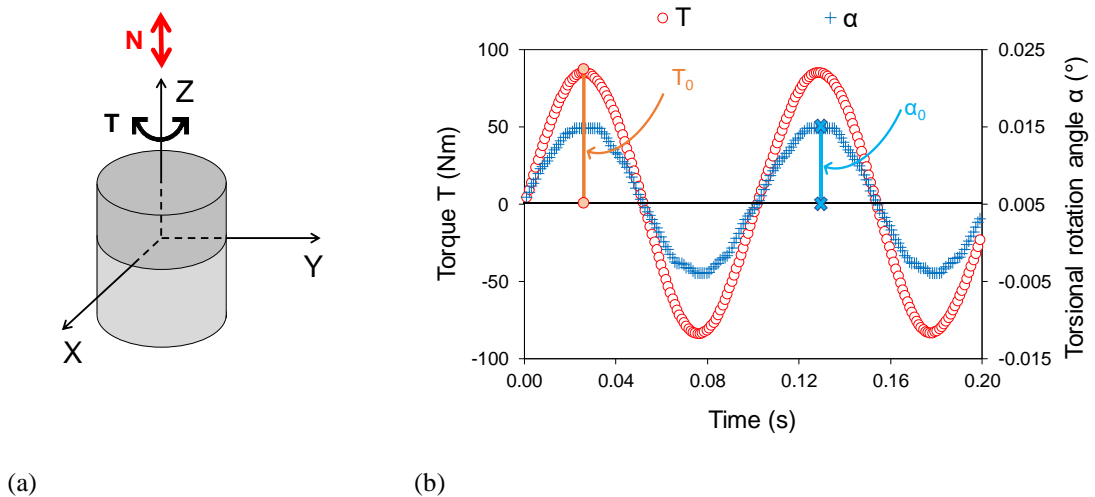


Fig. 4. Schematic representation of the test: (a) identification of the coordinate reference system and (b) set of recorded data.

Torque test on a cylindrical specimen generates shear stresses in XY plane equal to zero in the centre and maximum on the outer circumference. Assuming that the shear stress has a linear variation over the radius of the specimen, the maximum value τ_{max} is expressed by the following equation:

$$\tau_{max} = \frac{2T}{\pi R^3} \quad (1)$$

where T is the applied torque and R is the radius of the specimen.

For sinusoidal loading, $\tau_{max}(t)$ is given by the following equation:

$$\tau_{max}(t) = \tau_{max,0} \sin(\omega t) = \frac{2T_0}{\pi R^3} \sin(\omega t) \quad (2)$$

where T_0 is the amplitude of the applied torque, ω is the pulsation, equal to $2\pi f$ with f the load frequency, and t is the time.

The applied torque generates a maximum shear strain γ_{max} that can be calculated through the following equation:

$$\gamma_{max} = \frac{R\alpha}{H} \quad (3)$$

where H is the specimen height and α is the torsional rotation angle.

For sinusoidal loading, $\gamma_{max}(t)$ is given by the following equation:

$$\gamma_{max}(t) = \gamma_{max,0} \sin(\omega t - \varphi) = \frac{R}{H} \alpha_0 \sin(\omega t - \varphi) \quad (4)$$

where α_0 is the amplitude of the torsional rotation angle and φ is the phase angle, which is related to the time lag between stress and strain.

For a single layer homogeneous specimen, the complex shear modulus G^* is given by the following equation:

$$G^* = \frac{\tau_{max}^*}{\gamma_{max}^*} = \frac{\tau_{max,0} \exp[j\omega t]}{\gamma_{max,0} \exp[j(\omega t - \varphi)]} = |G^*| \exp[j\varphi] \quad (5)$$

where j is the imaginary unit and $|G^*|$ is the norm of the shear complex modulus.

By substituting Eqs. (2) and (4) into Eq. (5), G^* can be calculated through the following equation:

$$G^* = \frac{H}{I_p} \frac{T_0 \exp[j\omega t]}{\alpha_0 \exp[j(\omega t - \varphi)]} \quad (6)$$

where $I_p = \frac{\pi R^4}{2}$ is the polar moment of inertia of the circular section.

In the present study, G^* represents an equivalent complex shear modulus associated with the overall behaviour of the double-layered cylindrical specimen. Hence, in Eq. (6) $H = h_1 + h_2$ (Table 1). The change of this equivalent G^* was used as an indicator of fatigue damage. The amplitude of the torsional rotation angle α_0 also deserves some attention. Different from homogeneous specimens, where α_0 is given only by the mixture shear strain, for double-layered specimens α_0 is given by the contribution of the mixture shear strain and the interlayer shear strain.

3.2 Acoustic emission technique

During the fatigue test, AE signals were recorded using a Euro Physical Acoustics (EPA) system. AE signals were detected by eight piezoelectric transducers (miniature sensors Nano30), with an optimum operating frequency range of 125-750 kHz. As shown in Fig. 5, four transducers were mounted on the upper layer of the specimen (Plane U), whereas four transducers were mounted on the lower layer (Plane L). A silicon grease was applied between the sensors and the specimen in order to enhance the coupling and to reduce the loss of acoustic signal at the transducer-sample interface. AE signals were pre-amplified using four pre-amplifiers (IL40S model) with a 40 dB gain set in order to reduce noise (Fig. 6). AE signals were sampled at a rate of 20 MHz and filtered with an amplitude threshold of 40 dB. Therefore, a single AE event is defined as an AE signal that exceeds the threshold level, and it can be detected on several sensors.

The position where an AE event is generated is not known a priori. The location method is usually based on evaluating the differences of the time of arrival (TOA) of AE waves among the sensors placed on the surface of the specimen. Another important parameter required for the

location method is the wave propagation velocity. Detailed information on the adopted AE localisation method are described in Lamy et al. [16] and Diakhaté et al. [27].

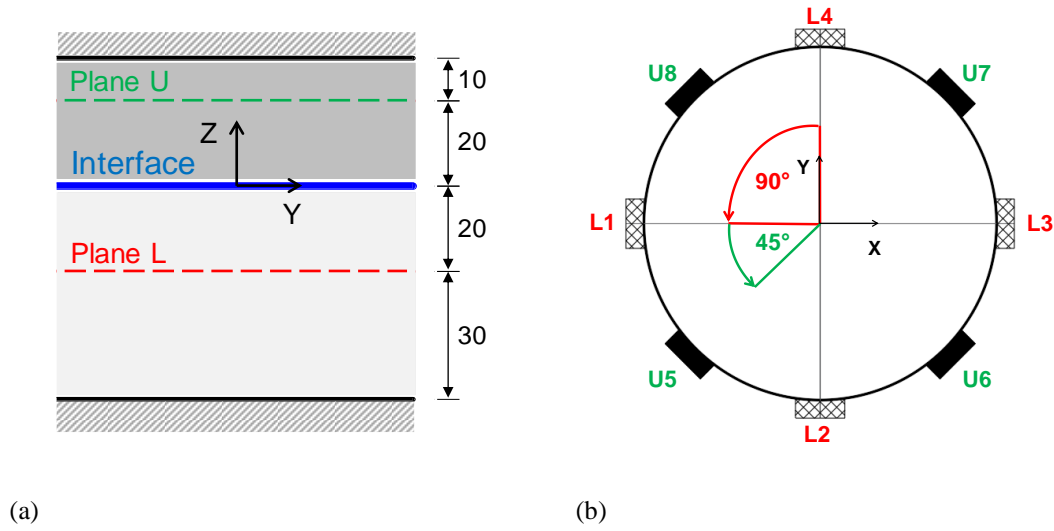


Fig. 5. Sections of the cylindrical specimen and piezoelectric transducers location: (a) vertical and (b) horizontal.

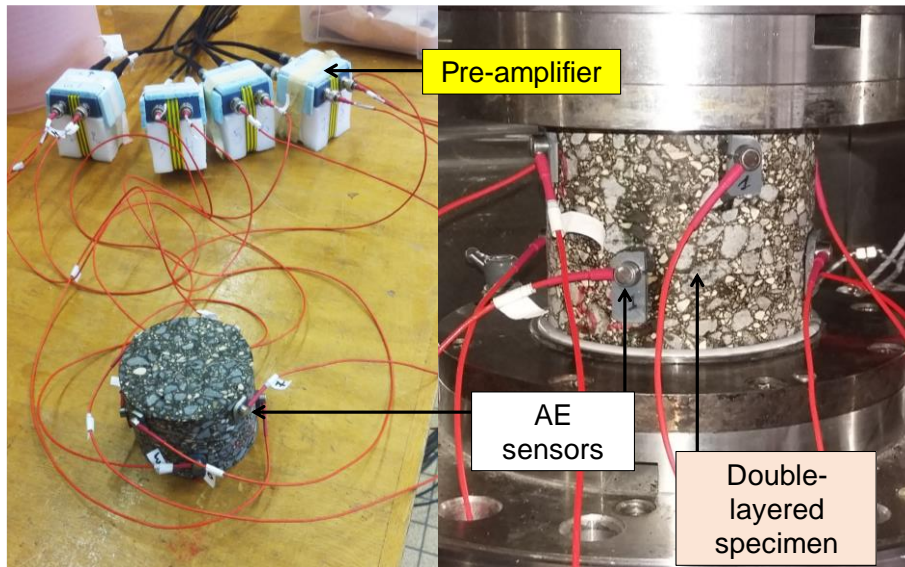


Fig. 6. AC specimen instrumented with acoustic emission sensors and pre-amplifiers.

In this study, the 3D localisation of the AE sources was improved by performing a calibration protocol called pencil lead break (PLB) test. This test consists in simulating an AE event using the fracture of a brittle graphite lead in a prefixed PLB position. This fracture generates an intense acoustic signal, quite similar to a natural AE source that the sensors detect as a strong burst. The PLB test was performed at the end of the shear-torque fatigue test on the

fractured surfaces of each specimen considering 13 points as shown in Fig. 7. Six pencil lead break repetitions were performed in each position.

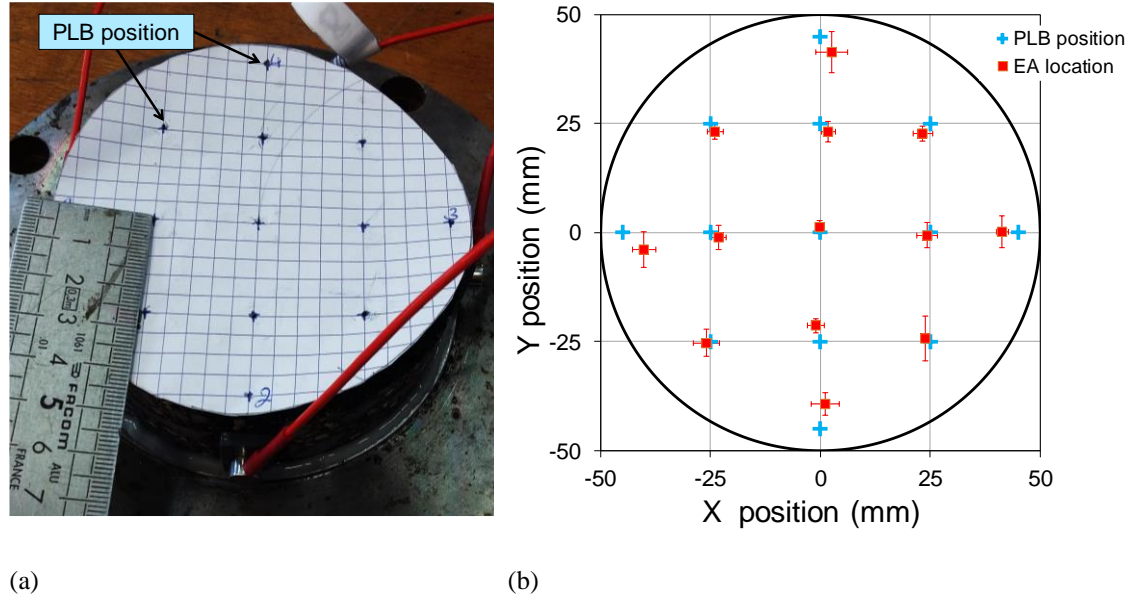


Fig. 7. Calibration of the AE-location with the PLB test: (a) square mesh of 25 mm overlaid on the fractured surface and (b) PLB test results.

Table 2. Average and standard deviation of the AE-locations.

PLB position (mm)		EA location			
		average (mm)		standard deviation (mm)	
X	Y	X	Y	X	Y
0	0	-0.30	1.33	0.74	1.50
0	-25	-0.95	-21.33	1.91	1.68
0	-45	1.15	-39.27	3.19	2.62
0	25	1.80	23.15	1.54	2.29
0	45	2.55	41.44	3.67	4.70
-45	0	-40.14	-3.97	2.68	4.08
-25	0	-23.09	-1.16	1.71	2.80
25	0	24.31	-0.57	2.35	2.82
45	0	41.39	0.29	1.41	3.66
25	25	23.27	22.75	2.25	1.65
-25	25	-23.99	23.25	1.84	1.91
25	-25	23.95	-24.33	1.15	5.18
-25	-25	-26.02	-25.23	2.97	3.09

The calibration results are shown in Fig. 7b and the data are summarised in Table 2. Dispersion in acoustic location was less significant in the centre of the fracture surface ($x = 0$ mm; $y = 0$ mm), and more significant closer the transducers.

The wave velocity was experimentally evaluated using the Auto Sensor Test (AST) protocol [16] by artificially generating short-duration and localised impulses, like the breaking of a pencil lead, at known distances from sensors. The average effective AE wave velocity through the AC specimens was measured equal to 3,500 m/s.

4. Results and discussion

4.1 Mechanical analysis

The cyclic torque applied during the test caused the progressive damage of the specimen, leading to a complete separation between the two layers at the end of the test. This mode of failure confirms that the interlayer is a zone of weakness in a double-layered specimen [31]. The damage evolution of the specimen was analysed using the normalised norm of complex shear modulus $|G^*|_n$ given by the following equation:

$$|G^*|_n = \frac{|G^*|_N}{|G^*|_0} \quad (7)$$

where $|G^*|_N$ is the norm of the complex shear modulus calculated at any given number of loading cycles (N), and $|G^*|_0$ is the initial norm of the complex shear modulus when the double-layered specimen is still not damaged.

Fig. 8 shows $|G^*|_n$ as a function of the number of loading cycles for the two tested specimens. As expected, $|G^*|_n$ decreases with the number of loading cycles and the number of loading cycles required to completely fracture the specimen (N_{\max}) increases with decreasing applied torque. Specimen 1 failed after 953,263 cycles and the evolution of $|G^*|_n$ was similar to that observed for asphalt concrete subjected to cyclic testing, where three typical stages can be normally observed [13, 32]. In the first stage, the complex modulus decreases rapidly, whereas, in the second stage, the complex modulus decreases quasi-linearly. Finally, the third stage is characterised by a quick decrease of complex modulus until the complete failure of the specimen. Specimen 2 failed after 61,150 cycles and different stages cannot be distinguished. This behaviour can be due to the higher applied torque. However, it is highlighted that specimen 2 was cored close to the corner of the slab. In this area, the presence of the rigid mould restricts

the movement of the aggregates close to the border (boundary effect) during the compaction. This generally results in differences in the internal aggregate structure of the material between the corners and the centre of the slab, and for this reason, the material could present lower mechanical performance [33, 34].

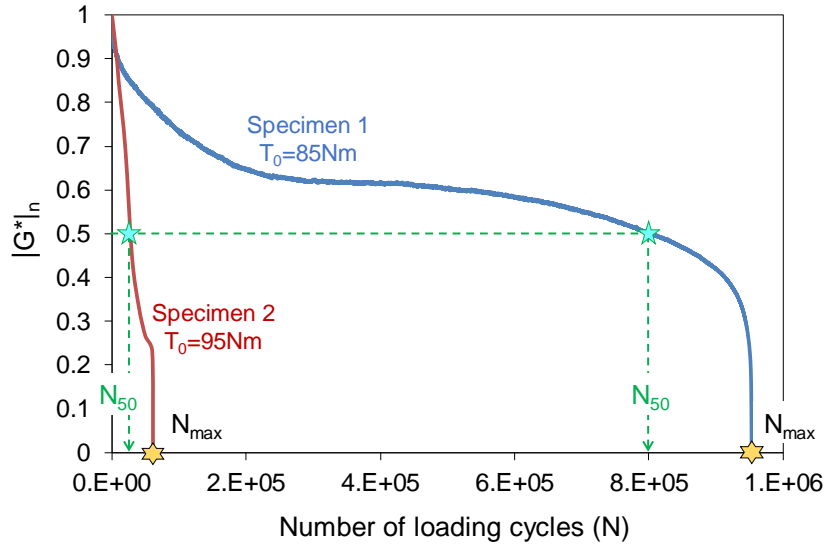


Fig. 8. Evolution of $|G^*|_n$ in shear-torque fatigue test at 10 Hz and 20 °C and classical fatigue failure criterion.

Mechanical behaviour of asphalt materials under cyclic load is very complex, and, in general, the decrease of $|G^*|_n$ is due to different phenomena (nonlinearity, heating, thixotropy and fatigue) that coexist and cannot be separated directly. In particular, some of these phenomena are reversible such as heating, thixotropy and recoverable nonlinearity (complex modulus dependency on stress/strain amplitude), whereas fatigue is irreversible and corresponds to the true damage [35, 36]. Since the cyclic torque tests were carried out on double-layered specimens, the complexity of the problem increases.

The fatigue life may be estimated by considering various failure criteria, and it is generally defined as the number of loading cycles to failure (N_f). The value N_f is lower than N_{max} and is usually associated with the number of loading cycles at which the initial modulus is reduced by a prefixed percentage (e.g. 50% $\rightarrow N_f = N_{50}$). As shown in Fig. 8, by referring to the classical fatigue failure criterion (N_{50}), the fatigue life for specimens 1 and 2 are of 800,000 and

30,000 cycles, respectively. This fatigue failure criterion does not provide any information on the localisation of the damage and is not able to distinguish if the damage occurs in the asphalt matrix or is localised at the interlayer.

4.2 Acoustic Analysis: 3D AE-localisation

The localisation of the AE event is fundamental to investigate the fracture mechanism evolution. Figs. 9 and 10 show the AE events (each dot represents an individual event recorded inside the specimen) projected onto the X-Z plane and Y-Z plane, respectively for specimens 1 and 2. The total number of events was higher for specimen 2 (about 500) compared to specimen 1 (about 170). In both specimens, AE events seem to be mostly located in the interlayer zone, which ultimately became the macro-crack leading to the complete failure of the specimen. Some AE events were located near the bottom and upper steel platens. This effect can be explained by the fact that in these areas the stress state is affected by the confinement effect (Poisson effect) due to the glueing. Besides, a certain number of points are also identified outside the specimen (in correspondence of the steel platens). This could be due to the uncertainties of the localisation method and/or because of echo events that generate position errors.

This behaviour was consistent for both specimens and confirms that AE analysis can be used to investigate the development of the damage process of asphalt materials.

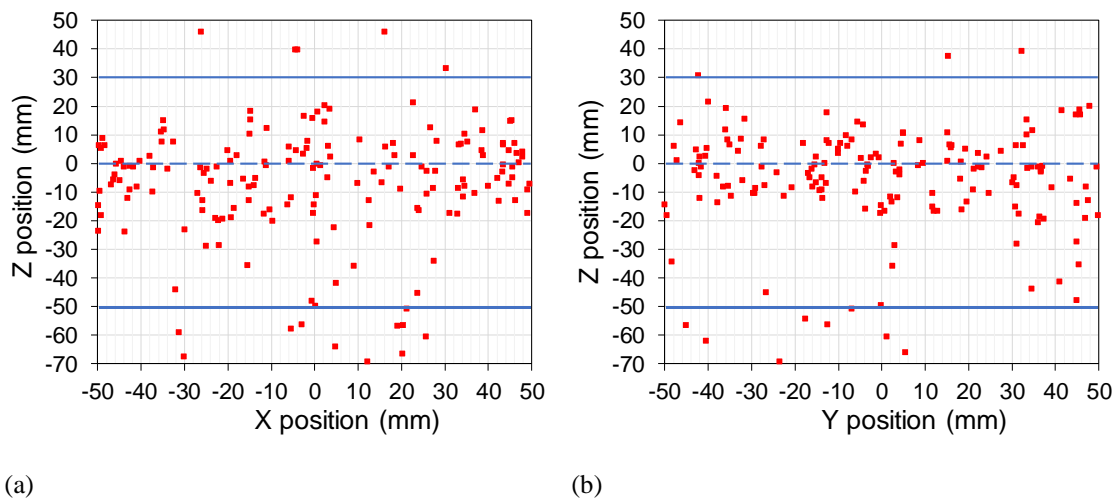


Fig. 9. Cumulated location of AE events for specimen 1: (a) X-Z plane, and (b) Y-Z plane.

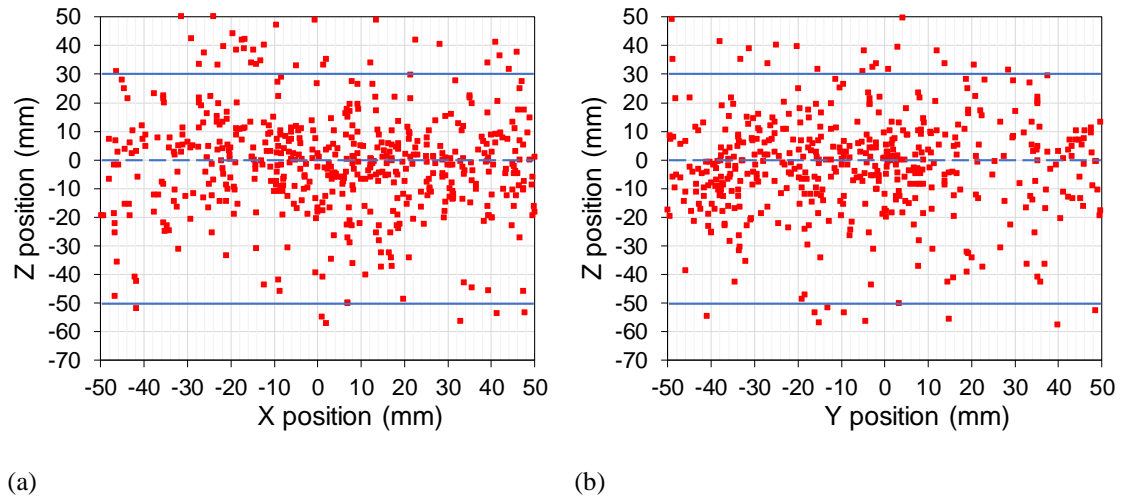


Fig. 10. Cumulated location of AE events for specimen 2: (a) X-Z plane, and (b) Y-Z plane.

In order to better understand the results obtained from the acoustic analysis, a statistical analysis was carried out. Figs. 11 and 12 show the frequency distribution along Z position of the EA events reported in Figs. 9 and 10, respectively. For both specimens, it can be observed that the EA events are mostly concentrated within the range -7.5 and +7.5 mm.

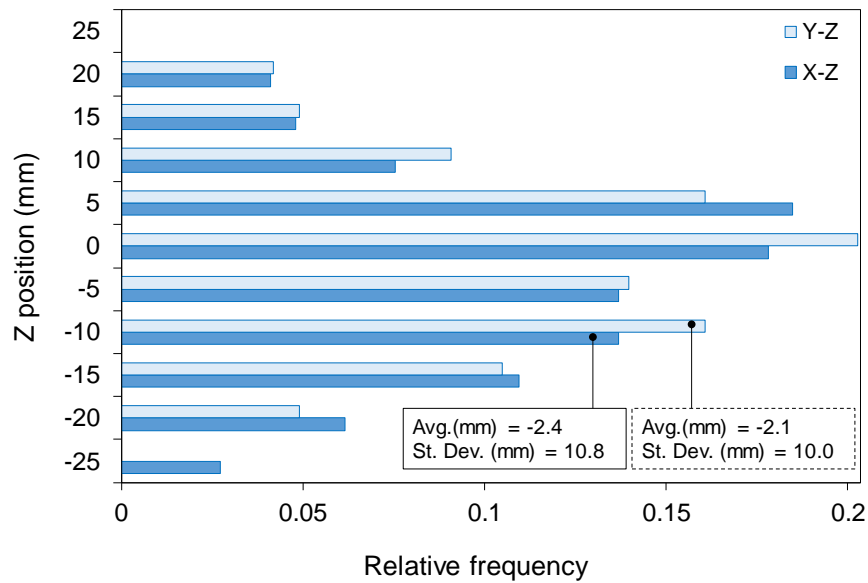


Fig. 11. EA events frequency distribution along Z position for specimen 1.

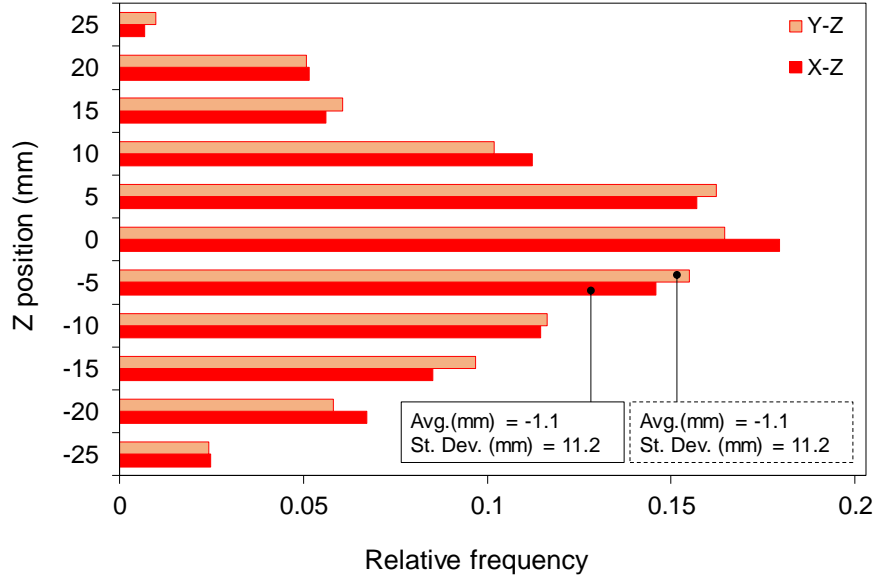


Fig. 12. EA events frequency distribution along Z position for specimen 2.

The statistical distribution of the measurements along the Z position was checked using a normal Quantile-Quantile (QQ) plot. Fig. 13 reports the data for both specimens in the X-Z and Y-Z planes. The points plotted along the equality line, confirming that most of the AE events may be considered normally distributed around the interface. The two tails outside the range -2 and +2 show a possible deviation from normality. These points can be related to the AE events located close to the steel platens which are not part of the same normal distribution. Thus, it is possible to affirm that the damage tends to localise in the interlayer zone, confirming that this is the weakest part of the specimen.

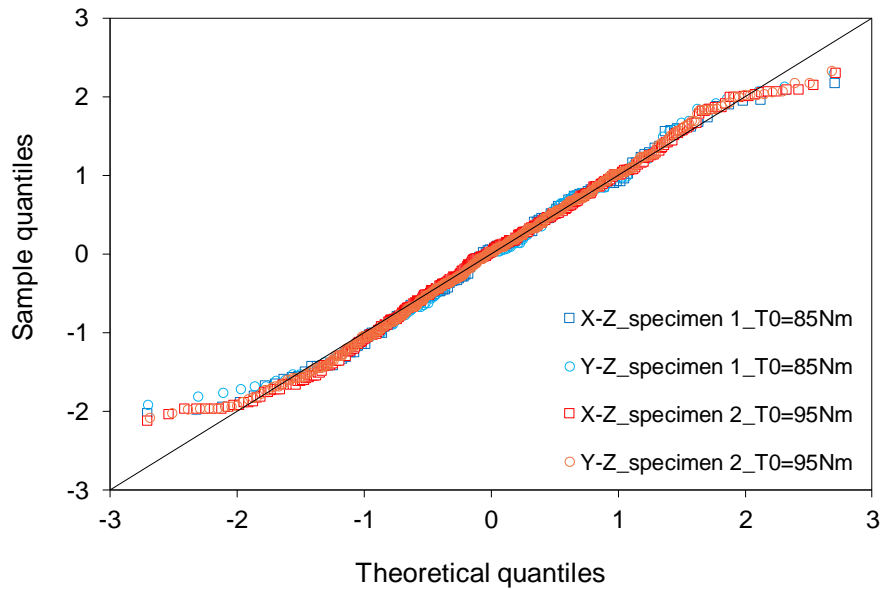


Fig. 13. Normal QQ plot of AE events along Z position for specimen 1 and specimen 2.

Fig. 14 presents the AE events on the X-Y plane for specimens 1 and 2 at the end of the test. The events are classified with the scale of the peak amplitude. It was observed during the tests that only AE events with small amplitudes occurred at the initial stage, and the events with large amplitudes began gradually to occur until reaching the peak at the end of the test. In Fig. 14, for both specimens, it can be observed that AE events were distributed mostly around the border of the specimen. A certain number of points were also identified outside the specimen. These events could be generated by uncertainties of the localisation method and/or because of echo events as already observed in Figs. 9 and 10.

A statistical analysis of the distribution of AE events on the X-Y plane was also carried out. The cross-section of each specimen was divided into four annuluses with the same area and with an outer radius equal to 25, 35.35, 43.3 and 50 mm, respectively. Fig. 15 shows the density of the EA events (number of events per unit area) reported in Fig. 14 as a function of the distance from the centre of the specimen ($R = \sqrt{X^2 + Y^2}$). The density was higher close to the circumference of the specimen, i.e. where the maximum shear stress occurs. Moreover, the cross-section of each specimen was also divided into eight sectors formed by angles of 45 degrees each. Fig. 16 shows the polar frequency distribution of the AE events reported in Fig. 14. The frequency of the events is not homogeneously distributed on the X-Y plane. These results agree with the previous observations and indicate that the AE events were mostly concentrated in certain areas.

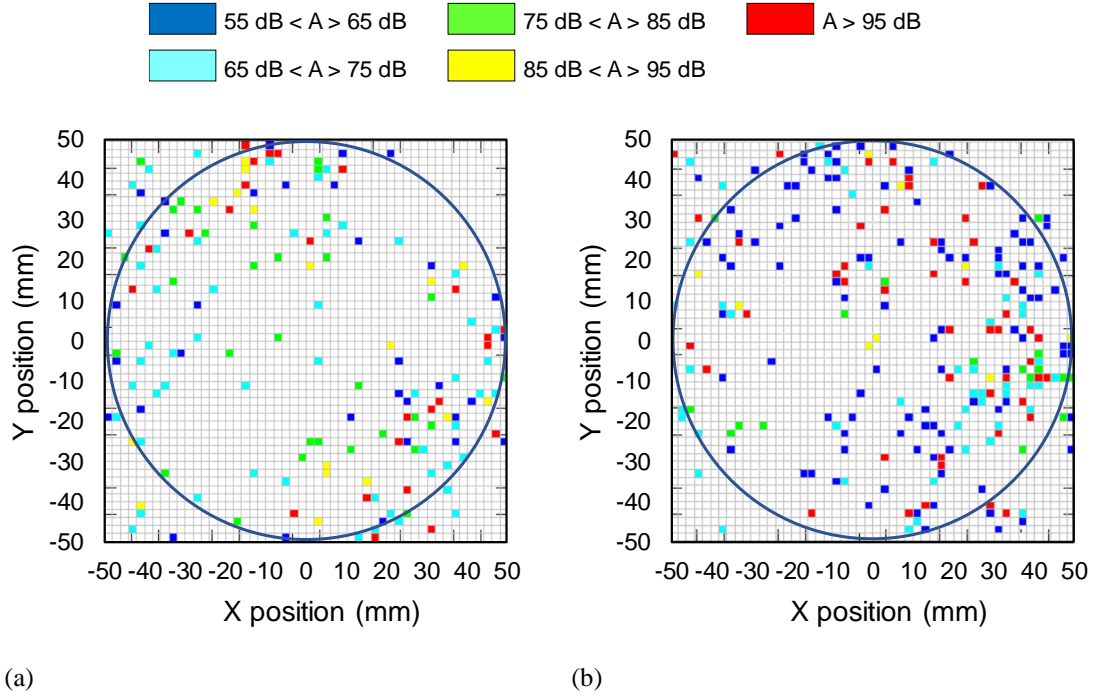


Fig. 14: Location of AE events on the X-Y plane: (a) specimen 1 and (b) specimen 2.

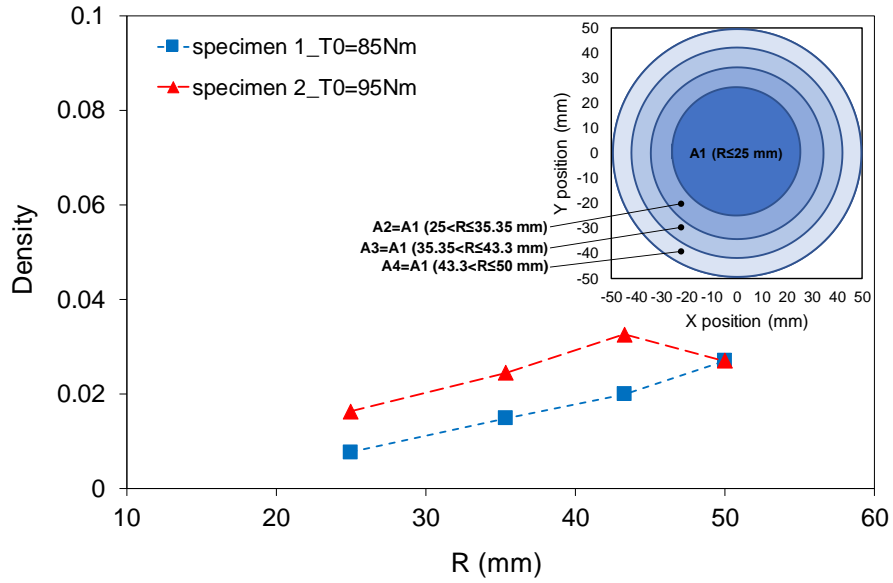


Fig. 15. EA events density on the X-Y plane as a function of the distance from the centre of the specimen (R) for specimen 1 and specimen 2.

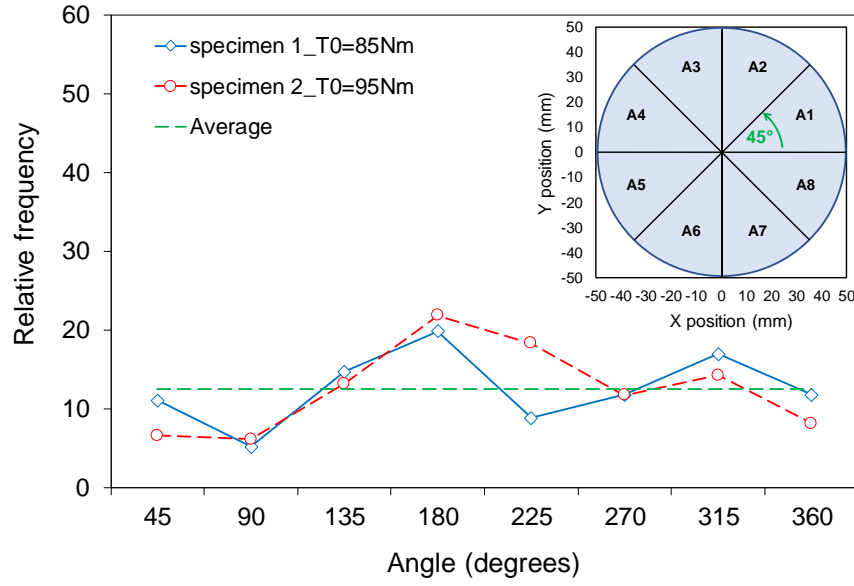


Fig. 16. EA events polar frequency distribution on the X-Y plane for specimen 1 and specimen 2.

4.3 Comparison between mechanical and AE results

Figs. 17 and 18 show the evolution of the cumulative number of AE events as a function of the number of loading cycles superposed to parameter $|G^*|_n$ for specimen 1 and specimen 2, respectively. Focusing on the evolution of the cumulative number of AE events, it is possible to identify two phases during the shear-torque fatigue test. A first phase during which the number of AE events increases almost linearly as the number of loading cycles increases. Subsequently, it can be observed a second phase during which the cumulative number rapidly increases as approaching the end of the test. Indeed, it is generally accepted that when the material is undamaged, the acoustic emission activity is almost negligible [15, 22]. The subsequent abrupt rise of AE activity indicates the formation of micro-cracks at the interlayer, as observed before, and occurs after 945,000 and 59,340 cycles for specimen 1 and 2, respectively, as shown in Figs. 17 and 18. This sharp increase of AE events, that corresponds to a rapid acceleration to failure, occurs when $|G^*|_n$ reaches approximately 30% for specimen 1 and 25% for specimen 2, i.e., when the complex shear modulus decreases by about 70%. Since acoustic activity is generally a sensitive precursor to the failure process [16, 18, 22, 37, 38], these results indicate that a huge part of the decrease is not accompanied by the formation of micro-cracks. These observations appear to be in strict agreement with those presented in a previous study [27].

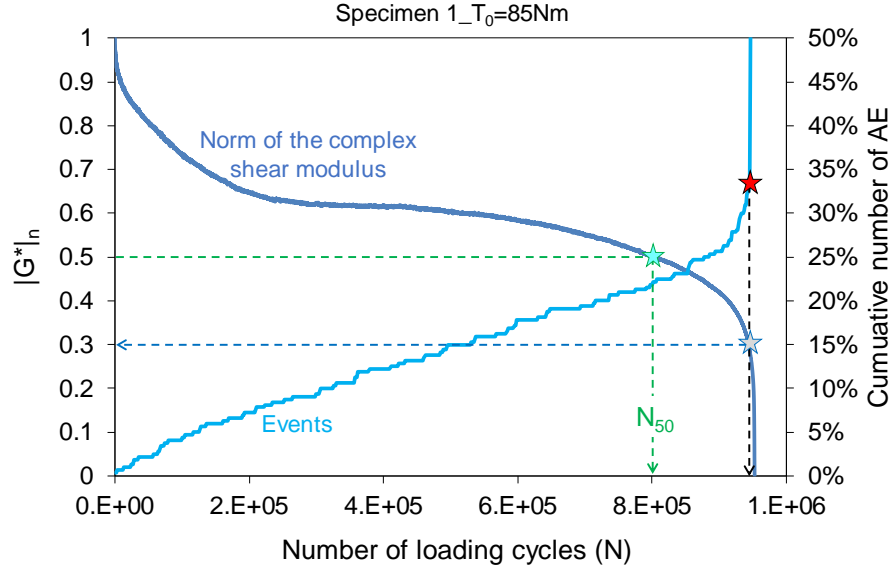


Fig. 17. Evolution of the cumulative number of AE events and of $|G^*|_n$ during shear-torque fatigue test for specimen 1.

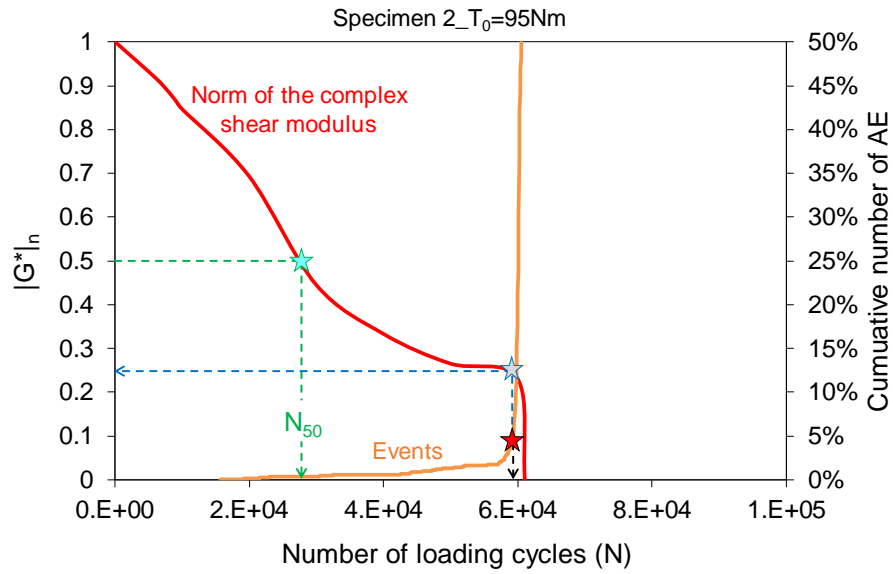


Fig. 18. Evolution of the cumulative number of AE events and of $|G^*|_n$ during shear-torque fatigue test for specimen 2.

A possible explanation is that, before the formation of the micro-cracks, the whole double-layered system reacts to the cyclic load. Thereafter, the damage tends to localise at the interlayer. Finally, the formation and propagation of macro-cracks at the interlayer leads to the complete separation of the two layers. Hence, it can be hypothesised that the $|G^*|_n$ evolution is

governed by the properties of the double-layered system at the beginning of the test, and progressively in a more pronounced way by the interlayer behaviour until the failure.

In this context, it is important to interpret the change in complex modulus during fatigue tests correctly. In fact, the term “damage” is typically referred to any microstructural change within the material that occur during a loading application. Considering that AE activity clearly represents the damage process of the AC specimen, this leads to conclude that asphalt pavement shear-fatigue life could not be estimated properly using the classical failure criterion (N_{50}). In fact, it could be argued that close to the 50% decrease of the parameter $|G^*|_n$, cracks do not begin to develop in the material or grow at undetectable rates. Therefore, it is helpful to develop a better failure criterion capable to evaluate the fatigue life during cyclic shear loading.

As a final remark, acoustic data and analysis can lead to further modelling and seem to be suitable for understanding and describing the failure mechanisms, as well as damage process during shear-fatigue behaviour.

5. Conclusion and perspectives

Shear-torque tests were used for the first time to assess the fatigue behaviour of asphalt pavement interlayers. During the test, an AE technique was used to evaluate the damage process leading to failure. The AE analysis included the cumulative number and the localisation of the AE events.

From the results, it can be concluded that:

- The shear complex modulus decreases with the number of cycles as a result of the deterioration of the interlayer mechanical properties.
- The AE analysis shows that the AE events are concentrated in the interlayer zone, where the specimen is weaker and where the failure actually occurs. Besides, the AE events are concentrated in the outermost of the cross-section area of the specimen, where the shear stress is higher. This allows concluding that the cracks initiate on the perimeter and proceeds inward.

- Comparing the results of both mechanical and AE analysis, the available data suggest that, despite an important “stiffness” decrease, the AE activity (formation of cracks) mainly occurs at the final stage of the test. The abrupt rise of AE events starts approximately when the corresponding decrease in the norm of complex modulus is approximately 70-75%. Thus, the results seem to indicate that the classical failure criterion (N_{50}) to predict asphalt pavement fatigue life, as usually proposed in the literature, does not seem to correspond to the critical damage condition of double-layered specimens and should be revised.

Although this work describes a preliminary experimental campaign, its outcome is very important for analysing and interpreting cyclic torque tests in asphalt mixtures. Thanks to the innovative use of AE analysis, the presented results can have an impact on the shear-fatigue characterisation of double-layered asphalt concrete systems, but they should be validated considering more data and different testing conditions.

References

- [1] Uzan J, Livneh M, Eshed Y. Investigation of adhesion properties between asphalt concrete layers. In: Proceedings of the Annual Meeting of the Association of Asphalt Paving Technologists; 1978. p. 495-521.
- [2] Al Nageim H, Al Hakim B. Bonding conditions between pavement layers and their influence on pavement layers moduli and remaining life. In: Proceedings of the 3rd European Symposium on Performance and Durability of Bituminous Materials and Hydraulic Stabilised Composites; 1999. p. 725–736.
- [3] Khweir K, Fordyce D. Influence of layer bonding on the prediction of pavement life. In: Proceedings of the Institution of Civil Engineers – Transport; 2003. p. 73–83.
<https://doi.org/10.1680/tran.2003.156.2.73>
- [4] Canestrari F, Ferrotti G, Lu X, Millien A, Partl MN, Petit C, Phelipot-Mardelé A, Piber H, Raab C. Mechanical testing of interlayer bonding in asphalt pavements. In: Partl M. et al. (eds)

Advances in interlaboratory testing and evaluation of bituminous materials. RILEM state-of-the-art reports 9; 2013. p. 303-360.

[5] Diakhaté M, Millien A, Petit C, Phelipot-Mardelé A, Pouteau B. Experimental investigation of tack coat fatigue performance: Towards an improved lifetime assessment of pavement structure interfaces. *Constr Build Mater* 2011;25:1123-1133.

<https://doi.org/10.1016/j.conbuildmat.2010.06.064>

[6] Zofka A, Maciej M, Alexander B, Ramandeep J, Audrius V, Rita K. Advanced shear tester for evaluation of asphalt concrete under constant normal stiffness conditions. *Road Mater Pavement Des* 2015;16:187–210. <https://doi.org/10.1080/14680629.2015.1029690>

[7] Song W, Shu X, Huang B, Woods M. Laboratory investigation of interlayer shear fatigue performance between open-graded friction course and underlying layer. *Constr Build Mater* 2016;115:381-389. <https://doi.org/10.1016/j.conbuildmat.2016.04.060>

[8] Ragni D, Graziani A, Canestrari F. Cyclic interlayer testing in bituminous pavements. In: *Proceedings of 7th International Conference on Bituminous Mixtures and Pavements*; 2019. p. 207-212. <https://doi.org/10.1201/9781351063265-31>

[9] Boudabbous M, Millien A, Petit C, Neji J. Energy approach for the fatigue of thermoviscoelastic materials: Application to asphalt materials in pavement surface layers. *Int J Fatigue* 2013;47:308–318. <https://doi.org/10.1016/j.ijfatigue.2012.09.013>

[10] Isailović I, Cannone Falchetto A, Wistuba M. Fatigue investigation on asphalt mixture layers' interface. *Road Mater Pavement Des* 2017;18(sup4):514-534.

<https://doi.org/10.1080/14680629.2017.1389087>

[11] Leutner R. Untersuchung des Schichtenverbundes beim bituminösen Oberbau. *Bitumen* 1979;41(3):84–91.

[12] Di Benedetto H, Ashayer S, Chaverot P. Fatigue damage for bituminous mixtures: a pertinent approach. *J Assoc Asphalt Paving Technol* 1996;65:142-158.

[13] Di Benedetto H, de La Roche C, Baaj H, Pronk A, Lundström R. Fatigue of bituminous mixtures. *Mater Struct* 2004;37:2002-2016. <https://doi.org/10.1007/BF02481620>

- [14] Brunner AJ, Howald MT, Niemz P. Acoustic emission rate behavior of laminated wood specimens under tensile loading. *J Acoust Emiss* 2006;24:104–110.
- [15] Chen Z, Gabbitas B, Hunt D. Monitoring the fracture of wood in torsion using acoustic emission. *J Mater Sci* 2006;41(12):3645-3655. <https://doi.org/10.1007/s10853-006-6292-6>
- [16] Lamy F, Takarli M, Angellier N, Dubois F, Pop O. Acoustic emission technique for fracture analysis in wood materials. *Int J Fract* 2015;192(1):57-70.
<https://doi.org/10.1007/s10704-014-9985-x>
- [17] Maji AK, Shah SP. Process zone and acoustic emission in concrete. *Exp Mech* 1988;28(1):27-33. <https://doi.org/10.1007/BF02328992>
- [18] Landis EN. Micro-macro fracture relationships and acoustic emissions in concrete. *Constr Build Mater* 1999;13:65-72. [https://doi.org/10.1016/S0950-0618\(99\)00009-4](https://doi.org/10.1016/S0950-0618(99)00009-4)
- [19] Shah SG, Ray S, Kishen JMC. Fatigue crack propagation at concrete–concrete bi-material interfaces. *Int J Fatigue* 2014;63:118-126. <https://doi.org/10.1016/j.ijfatigue.2014.01.015>
- [20] Prashanth MH, Singh P, Kishen JMC. Role of longitudinal reinforcement on the behavior of under reinforced concrete beams subjected to fatigue loading. *Int J Fatigue* 2019;125:271-290. <https://doi.org/10.1016/j.ijfatigue.2019.03.047>
- [21] Nesvijski E, Marasteanu M. Spectral analysis of acoustic emission of cold cracking asphalt. *E-J Nondestr Test Ultrasonics* 2006;11:10.
- [22] Behnia B, Buttlar W, Reis H. Evaluation of low-temperature cracking performance of asphalt pavements using acoustic emission: a review. *Appli Sci* 2018;8:306.
<https://doi.org/10.3390/app8020306>
- [23] Khosla NP, Goetz WH. Tensile characteristics of bituminous mixtures as affected by modified binders. Joint Highway Research Project. Purdue University and the Indiana State Highway Commission: West Lafayette, Indiana; 1979.
- [24] Hesp S, Terlouw T, Vonk W. Low temperature performance of SBS-modified asphalt mixes. *J Assoc Asphalt Paving Technol* 2000;69:540–573.
- [25] Seo Y, Kim YR. Using acoustic emission to monitor fatigue damage and healing in asphalt concrete. *KSCE J Civ Eng* 2008;2 (4):237-243. <https://doi.org/10.1007/s12205-008-0237-3>

- [26] Li X, Marasteanu M. The fracture process zone in asphalt mixture at low temperature. *Eng Fract Mech* 2010;77:1175–1190. <https://doi.org/10.1016/j.engfracmech.2010.02.018>
- [27] Diakhaté M, Larcher N, Takarli M, Angellier N, Petit C. Acoustic techniques for fatigue cracking mechanisms characterization in hot mix asphalt (HMA). In: Scarpas A., Kringos N., Al-Qadi I, A. L. (eds) 7th RILEM international conference on cracking in pavements, RILEM bookseries; 2012.
- [28] Petit C, Allou F, Millien A, Fakhari Terhani F, Dopeux J. Hot mix asphalt cyclic torque tests for viscoelastic bulk shear behaviour. In: 21th international conference on asphalt pavements, ISAP, Fortaleza, Brazil; 2018.
- [29] EN 12591. Bitumen and bituminous binders – Specifications for paving grade bitumens; 2009.
- [30] EN 12697-33. Bituminous mixtures – Test methods for hot mix asphalt – Part 33: specimen prepared by roller compactor; 2007.
- [31] Santagata FA, Partl MN, Ferrotti G, Canestrari F, Flisch A. Layer characteristics affecting interlayer shear resistance in flexible pavements. *J Assoc Asphalt Paving Technol* 2008;77:221–256.
- [32] Nguyen QT, Di Benedetto H, Sauzéat C. Determination of thermal properties of asphalt mixtures as another output from cyclic tension-compression test. *Road Mater Pavement Des* 2012;13(1):85-103. <https://doi.org/10.1080/14680629.2011.644082>
- [33] Masad E, Muhunthan B, Shashidhar N, Harman T. Quantifying laboratory compaction effects on the internal structure of asphalt concrete. *Transport Res Record: J Transport Res Board* 1999;1681:179-185. <https://doi.org/10.3141/1681-21>
- [34] Hunter EA, Airey GD, Collop AC. Aggregate orientation and segregation in laboratory-compacted asphalt samples. *Transport Res Record: J Transport Res Board* 2004;1891:8-15. <https://doi.org/10.3141/1891-02>
- [35] Di Benedetto H, Nguyen QT, Sauzéat C. Nonlinearity, heating, fatigue and thixotropy during cyclic loading of asphalt mixtures. *Road Mater Pavement Des* 2011;12(1):129-158. <https://doi.org/10.1080/14680629.2011.9690356>

- [36] Babadopulos LFAL, Orozco G, Sauzéat C, Di Benedetto H. Reversible phenomena and fatigue damage during cyclic loading and rest periods on bitumen. *Int J Fatigue* 2019;124:303-314. <https://doi.org/10.1016/j.ijfatigue.2019.03.008>
- [37] Bouchak M, Farrow IR, Bond IP, Rowland CW, Menan F. Acoustic emission energy as a fatigue damage parameter for CFRP composites. *Int J Fatigue* 2007;29:457-470. <https://doi.org/10.1016/j.ijfatigue.2006.05.009>
- [38] Unnthorsson R, Runarsson TP, Jonsson MT. Acoustic emission based fatigue failure criterion for CFRP. *Int J Fatigue* 2008;30:11-20. <https://doi.org/10.1016/j.ijfatigue.2007.02.024>